

# Governing Principles of Alginate Microparticle Synthesis with Centrifugal Forces

Huseyin Burak Eral,<sup>†,‡,#</sup> Eric R. Safai,<sup>§,#</sup> Bavand Keshavarz,<sup>||,#</sup> Jae Jung Kim,<sup>§</sup> Jisoek Lee,<sup>⊥</sup> and P. S. Doyle<sup>\*,§</sup>

<sup>†</sup>Process and Energy Department, Delft University of Technology, Delft 2628 CD, The Netherlands

<sup>‡</sup>Van't Hoff Laboratory for Physical and Colloid Chemistry, University of Utrecht, Utrecht 3512 JE, The Netherlands

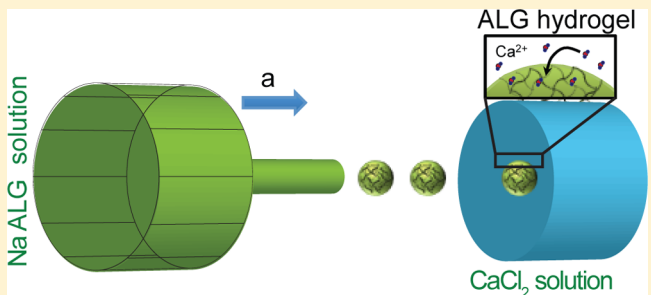
<sup>§</sup>Department of Chemical Engineering, Massachusetts Institute of Technology, Cambridge, Massachusetts 02139, United States

<sup>||</sup>Department of Mechanical Engineering, Massachusetts Institute of Technology, Cambridge, Massachusetts 02139, United States

<sup>⊥</sup>School of Energy and Chemical Engineering, Ulsan National Institute of Science and Technology, Ulsan 44919, Korea

## Supporting Information

**ABSTRACT:** A controlled synthesis of polymeric particles is becoming increasingly important because of emerging applications ranging from medical diagnostics to self-assembly. Centrifugal synthesis of hydrogel microparticles is a promising method, combining rapid particle synthesis and the ease of manufacturing with readily available laboratory equipment. This method utilizes centrifugal forces to extrude an aqueous polymer solution, sodium alginate (NaALG) through a nozzle. The extruded solution forms droplets that quickly cross-link upon contact with aqueous calcium chloride (CaCl<sub>2</sub>) solution to form hydrogel particles. The size distribution of hydrogel particles is dictated by the pinch-off behavior of the extruded solution through a balance of inertial, viscous, and surface tension stresses. We identify the parameters dictating the particle size and provide a numerical correlation predicting the average particle size. Furthermore, we create a phase map identifying different pinch-off regimes (*dripping without satellites*, *dripping with satellites*, and *jetting*), explaining the corresponding particle size distributions, and present scaling arguments predicting the transition between regimes. By shedding light on the underlying physics, this study enables the rational design and operation of particle synthesis by centrifugal forces.



## INTRODUCTION

With the development<sup>1</sup> of the nanotechnology and bioengineering fields, interest in controlled synthesis of polymeric particles has seen a rapid resurgence.<sup>2,3</sup> Applications ranging from medical diagnostics<sup>4</sup> to anticounterfeiting technologies<sup>5</sup> constantly challenge our capacity to produce polymeric particles efficiently.<sup>6</sup> In response, scientists and engineers have developed creative methods to synthesize polymeric particles<sup>7</sup> and to assemble them into more complex structures.<sup>8</sup> Microfluidics<sup>9–12</sup> and batch synthesis approaches<sup>13</sup> are the most commonly used synthesis methods. A directed assembly into more complex particles is achieved by external fields such as magnetic, electric, and hydrodynamic<sup>14,15</sup> as well as through asymmetric particle–particle interactions.<sup>16</sup> Applications place emphasis on various aspects of controlled synthesis of polymeric particles. Self-assembly studies require monodisperse building blocks with well-defined geometries, whereas medical and pharmaceutical applications place strict biocompatibility restrictions on the materials and synthesis methods used.<sup>2,3,17</sup>

Polymeric particles manufactured using natural biopolymers have recently risen to prominence in biological and pharmaceutical applications.<sup>18,19</sup> The biocompatibility, abun-

dance, and low-cost of natural polymers are the driving force behind this rapid expansion. Particularly, natural polymers, such as sodium alginate (NaALG),  $\kappa$ -carrageenan, and carboxymethylcellulose, that can cross-link to form hydrogels have been widely used in numerous applications such as controlled release of actives, encapsulation of biomolecules, and scaffolding for cell culture.<sup>20,21</sup> Notably, Lacy et al. used alginate (ALG) hydrogels to encapsulate islet cells capable of releasing insulin.<sup>22</sup>

Lab-scale synthesis of ALG hydrogel particles and fibers has been demonstrated using dripping,<sup>23–26</sup> coextrusion,<sup>27</sup> microfluidics,<sup>24,28,29</sup> inkjet printing, and 3D printing.<sup>20,21</sup> Bremond et al. also demonstrated encapsulation with very thin controlled layers of ALG hydrogels.<sup>27</sup> However, alternative methods capable of producing relatively large amounts of particles with standard lab equipment are still sought after. Among the aforementioned methods, centrifugal synthesis of ALG and chitosan hydrogels<sup>30,31</sup> has attracted interest because of its

Received: March 16, 2016

Revised: June 10, 2016

Published: June 16, 2016

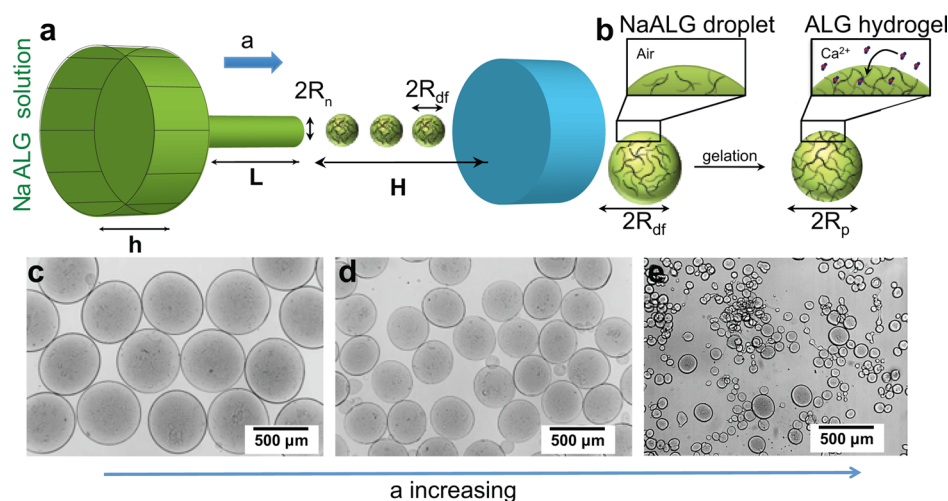


**Figure 1.** (a) Illustration of the experimental setup. Noncross-linked NaALG solution is extruded from a syringe nozzle of radius  $R_n$  by centrifugal acceleration  $a$ , forming droplets of radius  $R_d$ . The droplets cross-link and form hydrogels upon impact into the liquid bath. (b) Illustration of the gelation process where  $\text{Ca}^{2+}$  ions react with ALG to form hydrogels. Snapshots of ALG hydrogels produced at different accelerations where the concentration of NaALG is 3% wt/wt NaALG is extruded at (c) 1000, (d) 1500, and (e) 2200 rpm.

ability to produce large amounts of hydrogel microparticles, low-cost nature, and ease of implementation with readily available lab equipment (centrifuge, needle, and falcon tube). Compared with the standard dripping method that requires a pump, the centrifugal synthesis method provides an alternative means to overcome pressure drops with standard lab equipment. In this approach, the centrifugal force is used to extrude an aqueous NaALG solution through a nozzle of radius  $R_n$ . The NaALG solution either pinches off and breaks into droplets or forms a jet after extrusion from the nozzle depending on the balance of capillary, inertial, and viscous forces. The aqueous NaALG droplets quickly cross-link upon contact with aqueous calcium chloride ( $\text{CaCl}_2$ ) solution to form ALG hydrogel particles (Figure 1). The size distribution of hydrogel particles is controlled by the dynamics of the pinch-off and the cross-linking process in  $\text{CaCl}_2$  solution.

The centrifugal synthesis approach has been used to synthesize ALG hydrogel particles of various sizes and compositions for a variety of applications.<sup>32,33</sup> Lee and Kim synthesized composite ALG particles containing polydiacetylene liposomes for multitargeting.<sup>32</sup> Maeda et al. demonstrated the synthesis of composite particles and compartmentalized encapsulation of different moieties such as cells and composite magnetic colloids using multiple glass capillaries stacked together.<sup>33</sup> However, all of these efforts have focused on synthesizing ALG hydrogels empirically without providing an in-depth understanding of the phenomenon. Haeberle et al. used stroboscopic imaging techniques to visualize the pinch-off process under acceleration.<sup>34</sup> These authors provided stroboscopic images of filament formation and pinch-off along with reports on size distribution.

In all of the aforementioned studies, predicted sizes of synthesized hydrogel particles are based on a static force balance on a pendant droplet, Tate's law.<sup>35</sup> This static approach ignores the pinch-off phenomenon.<sup>36</sup> Studies on centrifugal synthesis have so far focused on demonstrating the versatility of the technique. The lack of physical understanding of the process limits the repeatability of previous work, as well as generalization of centrifugal synthesis to other materials.

In this study, a systematic analysis of the centrifugal hydrogel microparticle synthesis process for predicting (i) the particle

size and (ii) the pinch-off regimes is provided. The data collection is performed by measuring the average size and size distributions of cross-linked hydrogels by optical microscopy under various experimental conditions. Experimental parameters dictating the size of the hydrogel particles are identified, and a correlation predicting the average hydrogel particle size is presented. The proposed correlation takes into account the previously overlooked pinch-off phenomenon, and it is accurate within the *dripping without satellites* regime. On the basis of the observation of particle size distributions shown in Figure 1c–e, we develop scaling arguments explaining the emergence of different pinch-off regimes (*dripping without satellites*, *dripping with satellites*, and *jetting*). Incorporating the pinch-off process into the physical model of centrifugal synthesis enables a better understanding of the previously overlooked experimental parameters such as the viscosity of the extruded solution, length of the nozzle, and height of the fluid. This improved physical understanding of the process can aid in rational design of experiments and opens the possibility of expanding the centrifugal method into other polymeric materials. Utilizing the physical insights of our study, we provide a step-by-step guide aimed to help scientists in designing experiments in the Supporting Information.

## MATERIALS AND METHODS

**Chemicals and Materials.** NaALG (CAS: 9005-38-3),  $\text{CaCl}_2$  (CAS: 10043-52-4), sodium dodecyl sulfate (SDS, CAS: 151-21-3), Kolliphor P188 (KP188, CAS: 151-21-3), sodium hydroxide (NaOH, CAS: 1310-73-2), and trichloro(1H,1H,2H,2H-perfluorooctyl)silane (perfluorosilane, CAS: 78560-45-9) were purchased from Sigma Aldrich. All chemicals were used without any further treatment or modification. Blunt-end syringe nozzles of gauges (G) 21, 23, 25, and 30 were purchased from Nordson, with inner radii ( $R_n$ ) of 258, 168, 130, and 80  $\mu\text{m}$ , respectively. The length of the blunt nozzles  $L$  was 1.8 cm. All nozzles used in the study were made of stainless steel and were unmodified unless specified. Centrifugation was achieved with a tabletop, swinging bucket centrifuge (Eppendorf 5702).

**Experimental Procedure.** A schematic of the experimental setup is shown in Figure 1. NaALG droplets are generated through stainless steel blunt-tip needles of varying gauges by centrifugal force. A range of centrifugal accelerations (1–500 g) drives fluid flow, with the accelerated NaALG solution impacting a 500 mM  $\text{CaCl}_2$  bath. The

cross-linking of the NaALG polymer to form ALG hydrogels occurs upon impact on the  $\text{CaCl}_2$  bath. Resulting hydrogel particles are analyzed by image processing.

#### Fabrication of the Nozzle-In-Centrifuge (NiC) Apparatus.

Falcon tubes, 50 mL, are utilized as supports (outer chamber) for the syringe and needle (inner chamber) while also serving as the  $\text{CaCl}_2$  bath. The volume of the liquid in the  $\text{CaCl}_2$  bath is used to adjust the distance between the needle tip and the  $\text{CaCl}_2$  bath ( $H$ ). Syringes (10 mL) are cut to shape by hand and secured through a punctured tube cap using a hot melt adhesive to maintain needle positioning. This NiC apparatus provides accessibility to interchange the needle tip and all component specifications. The assembly and operation of the NiC apparatus are detailed in the [Supporting Information](#).

**Needle Silanization.** To hydrophobize the nozzle, untreated blunt needles were soaked in 1 M NaOH solution for 1 h. They were then dried with compressed argon. The needles were coated with perfluorosilane under vacuum with an incubation time of 2 h. The hydrophobicity was confirmed using bright field microscopy ([Supporting Information](#)).

**Droplet Generation and Observation.** NaALG solutions were prepared by mixing appropriate amounts of NaALG powder in water and subsequently stirring using a magnetic bar. Higher concentrations required longer agitation times to achieve homogeneous solutions. All solutions were prepared at room temperature. ALG and  $\text{CaCl}_2$  solutions were injected into the inner and outer chambers, 2 and 8 mL, respectively, prior to centrifugation. The cap securing the NaALG-containing syringe and nozzle was fixed at a height such that the distance  $H$  between the nozzle tip and the  $\text{CaCl}_2$  bath was 3.6 mm. The length of needles,  $L$ , used as the nozzle was 18 mm, and the distance,  $H$ , was kept constant at 3.6 mm throughout the study. The impact of varying  $H$  is elaborated in the [Supporting Information](#). Centrifugation times ranged from <30 to 60 s. Sub-thirty second spin times were used for less viscous NaALG solutions to minimize changes in  $H$ . NaALG concentrations varied between 0.5 and 8% wt/wt, with 2.5% wt/wt being our canonical solution. SDS was used to modify the surface tension of NaALG solutions.

Cross-linked hydrogel microparticles were maintained in  $\text{CaCl}_2$  solution prior to and during imaging. ALG microparticles were collected and imaged under bright field via an inverted microscope (Axiovert 200, Zeiss) equipped with a Nikon lens (2X to 20X). Images were processed using public domain software ImageJ (NIH) and a custom code was written in Matlab.

## RESULTS

The centrifugal microparticle synthesis process can be divided into two distinct phenomena: pinch-off and impact with the reaction ([Figures 1 and 3](#)). In pinch-off, NaALG solution exits the nozzle and forms a stream of droplets with radius  $R_{\text{df}}$  as a result of the balance between surface tension, inertial, and viscous forces. In the impact with the reaction stage, the impacting droplets penetrate into the  $\text{CaCl}_2$  bath. NaALG droplets solidify into ALG hydrogel microparticles with radius  $R_p$  because of the reaction of NaALG with the divalent cation  $\text{Ca}^{2+}$  ([Figure 1b](#)).<sup>37</sup> The focus of this study will be the pinch-off process where the centrifugal acceleration drives the flow of the fluid through the nozzle. We systematically investigate the factors dictating the hydrogel microparticle size ( $R_p$ ) and the pinch-off regimes governing the microparticle size distributions shown in [Figure 1c–e](#).

**Dimensional Analysis.** We first discuss factors dictating the formation and the size of the droplets during pinch-off through dimensional analysis using the Buckingham-Pi theorem<sup>38</sup> where  $\rho$ ,  $\gamma$ , and  $\mu$  are the fluid properties: density, surface tension, and viscosity of the extruded fluid, respectively.  $R_p$  is the particle radius, and  $R_n$  is the nozzle outer radius.  $\theta$  is the contact angle.  $U$  is the fluid velocity at the nozzle outlet,  $h$  is the height of the liquid, and  $L$  is the length of the nozzle

([Figure 1](#)). The dimensionless parameters pertinent to this study are

$$\begin{aligned} \frac{R_p}{R_n} &= f\left(Bo, We, Oh, \theta, \frac{h}{L}, \frac{L}{R_n}\right) \\ Bo &= \frac{\rho a R_n^2}{\gamma} \\ We &= \frac{\rho U^2 R_n}{\gamma} \\ Oh &= \frac{\mu}{\sqrt{\rho R_n \gamma}} \end{aligned} \quad (1)$$

where  $Bo$  stands for the Bond number, which captures the relative strength of gravitational stress imposed by the acceleration to capillary stress.  $We$  is the Weber number, which is the ratio of inertial and surface tension stresses. The Ohnesorge number,  $Oh$ , relates the viscous stress to inertia and surface tension stresses.<sup>39,40</sup>  $\theta$  is the advancing contact angle at the solid–liquid–gas interface formed by the nozzle, ALG solution, and air. The geometric parameters  $h/L$  and  $L/R_n$  are also important in determining the speed of flow inside of the nozzle.

The dimensional analysis suggests that the relative radius of the extruded droplet ( $R_d/R_n$ ) might depend not only on the balance of the surface tension force with the centrifugal body force as previously mentioned in the literature<sup>33,34</sup> but also on inertial and viscous forces. Furthermore, it suggests that previously overlooked parameters such as  $\theta$ ,  $h/L$ , and  $L/R_n$  can play a role in controlling  $R_d$ . Upon pinch-off, the droplet impacts the  $\text{CaCl}_2$  bath and assumes the final size  $R_p$  as shown in [Figure 1](#).

**Derivation of Flow Inside of the Nozzle.** The flow speed of the fluid while exiting the nozzle needs to be calculated to account for the inertial effects. The NaALG solution is extruded by the pressure head created by the centrifugal force ( $a$ ) acting on the total height of the fluid ( $h + L$ ). This problem is a special case for the pressure drop in inclined pipes where the driving force is the centrifugal force.<sup>38</sup> The majority of pressure drop occurs within the nozzle; we can assume a Hagen–Poiseuille form where spatially averaged velocity of the fluid at the nozzle outlet is

$$U = \frac{\rho a (h + L) R_{\text{ni}}^2}{8\mu L} \quad (2)$$

[Equation 2](#) is valid in the laminar flow regime where the Reynolds ( $Re$ ) number is smaller than 2000.  $R_{\text{ni}}$  is the inner radius of the nozzle. The Reynolds number is defined as  $Re = \rho U R_{\text{ni}} / \mu$  where  $\rho$  and  $\mu$  are the density and the viscosity of NaALG solution, respectively. For all of the experiments conducted in this study,  $Re$  is less than ten.

**Static Force Balance on a Pendant Drop.** A simple force balance can be written around the droplet and the nozzle where surface tension is balanced by the weight of the droplet. The surface tension force holding a pendant droplet ([Figure 3](#)) is  $2\pi R_n \gamma$ , and the weight of the droplet is  $4\pi R_{\text{di}}^3 \rho a / 3$ . This simple force balance is called Tate's law.<sup>35</sup>  $R_n$  and  $R_{\text{di}}$  are the outer radius of the nozzle and radius of the pendant drop. It is important to note that Tate's law is only applicable to pendant droplets, and it ignores the pinch-off process. Tate's law can be rewritten in a dimensionless form as

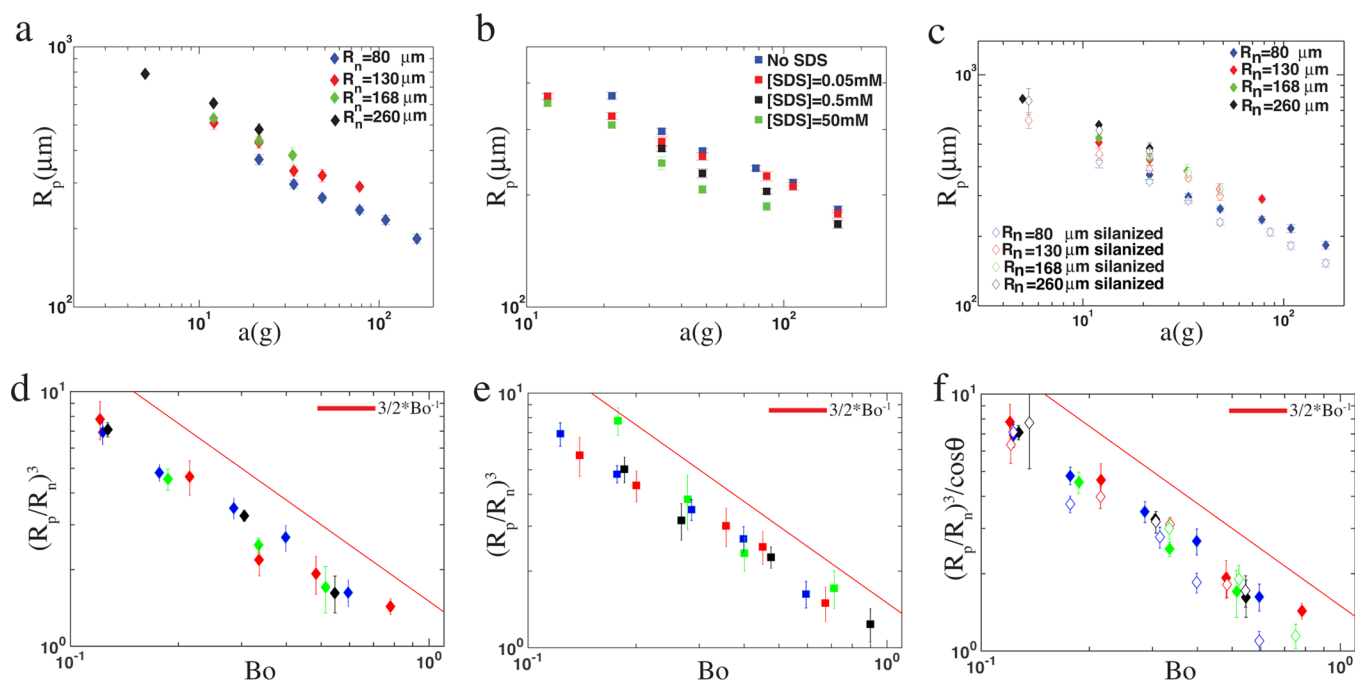


**Figure 2.** (a) Effect of the nozzle size on the hydrogel particle size: radius of hydrogel particles ( $R_p$ ) versus centrifugal acceleration ( $a$ ) produced with four different nozzle radii ( $R_n$ ). (b) Effect of surface tension: radius of hydrogel particles produced by extruding noncross-linked ALG solutions with different surfactant concentrations vs centrifugal acceleration ( $a$ ). (c) Effect of the contact angle: radius of hydrogel particles ( $R_p$ ) produced with hydrophobic (silanized)  $\theta \approx 100^\circ$  and hydrophilic (untreated) nozzles ( $\theta \approx 0^\circ$ ) vs centrifugal acceleration. (d) Dimensionless particle radius cubed vs Bond number ( $Bo$ ) for different radii nozzles given in panel a. (e) Dimensionless particle radius cubed vs  $Bo$  for ALG solutions with different surface tensions given in panel b. (f) Dimensionless particle radius cubed divided by  $\cos \theta$  vs  $Bo$  for hydrophobic and hydrophilic surfaces given in panel f. The presented data are obtained with the canonical sample 2% NaALG, and they are limited to the *dripping without satellites* regime.

$$\left(\frac{R_{\text{di}}}{R_n}\right)^3 = \frac{3}{2}Bo^{-1} \quad (3)$$

The effect of the contact angle can be introduced into Tate's law by incorporating the contact angle into the surface tension force, holding the pendant droplet ( $2\pi R_n \gamma \cos \theta$ ) against the weight of the droplet, which is  $4/3\pi R_{\text{di}}^3 \rho a$ . This equation can be rewritten in a dimensionless form as

$$\left(\frac{R_{\text{di}}}{R_n}\right)^3 \frac{1}{\cos \theta} = \frac{3}{2}Bo^{-1} \quad (4)$$

**Estimating the Size of Hydrogel Particles.** The resulting hydrogel particle size is arguably the most important parameter in centrifugal hydrogel microparticle synthesis. For biomedical and drug delivery applications, the size dictates the time scale of mass transport of actives through diffusion along with network properties such as mesh size.<sup>25,26</sup> Dimensional analysis discussed in the **Dimensional Analysis** section indicates that the relative size of the pinched-off droplet normalized by the nozzle radius might have a dependency on dimensionless numbers,  $Bo$ ,  $We$ , and  $Oh$ , and  $\theta$  as well as other geometric factors given in eq 1.

In Figure 2, we systematically investigate the effect of acceleration ( $a$ ), outer nozzle radius ( $R_n$ ), surface tension ( $\gamma$ ), and contact angle ( $\theta$ ) on the hydrogel particle size ( $R_p$ ) while keeping the viscosity of NaALG solution and other geometric factors in eq 1 constant. In Figure 2a,  $R_p$  is plotted against the acceleration for four different nozzle sizes ( $R_n$ ). Two trends appear in Figure 2a.  $R_p$  decreases with decreasing nozzle radius,  $R_n$ , and with increasing acceleration. Furthermore, below a certain acceleration, centrifugal synthesis did not produce

droplets (discussed in the **No-Dripping to Dripping Transition** section). Above a critical acceleration, satellite droplets and broad droplet size distributions were observed (Figure 1d,e). We excluded the data points where satellites and broad distributions are observed in Figures 2 and 3. The emergence of aforementioned heterogeneous size distributions is discussed in sections below.

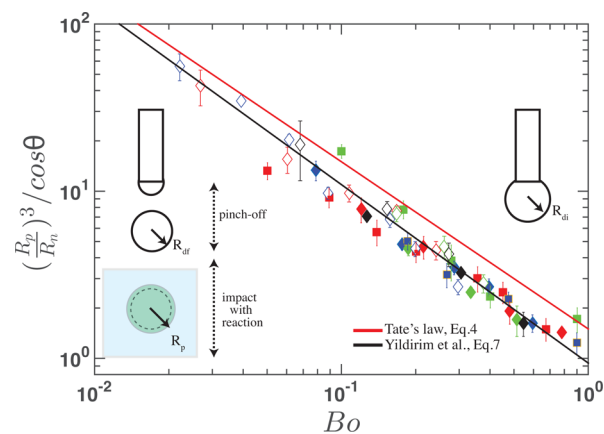


**Figure 3.** Ratio of the particle radius ( $R_p$ ) to the nozzle radius ( $R_n$ ) cubed divided by  $\cos \theta$  at different Bond numbers ( $Bo$ ) for different nozzle sizes, surfactant concentrations, and surface treatments. The lines are Tate's law<sup>35</sup> (eq 3, red line) and the numerical prediction from Yildirim et al.<sup>43</sup> (eq 6, black solid line). The presented data are limited to the *dripping without satellites* regime for the canonical sample. In the inset image, dotted green line indicates swelling/shrinking upon cross-linking.

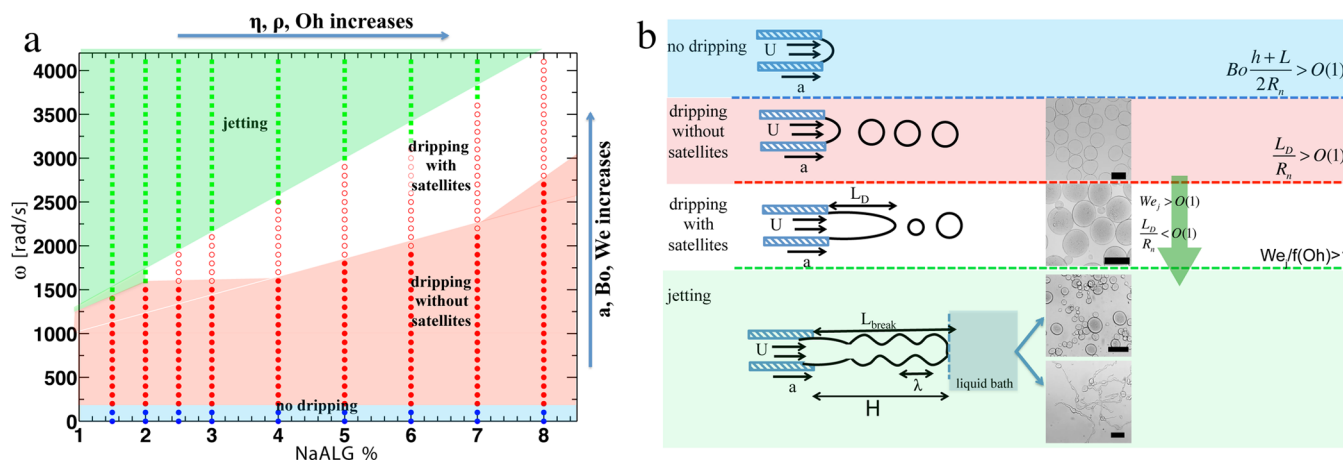


**Figure 4.** (a) Experimental phase diagram showing different pinch-off regimes as a function of centrifugal speed ( $\omega$ ) and NaALG concentration by weight (NaALG%) for a nozzle size of  $R_n = 80 \mu\text{m}$ . (b) Illustrations of different pinch-off regimes with resulting hydrogel formations and summary of conditions for transitions between different regimes. The thick green arrow indicates the transition between *dripping without satellites* to *jetting* regimes without entering the *dripping without satellites* regime.

The effect of surface tension on the size of hydrogel particles is shown in Figure 2b for  $R_n$  fixed at  $80 \mu\text{m}$ . Increasing the surfactant concentration decreases the surface tension (Supporting Information), which leads to smaller droplets. Figure 2c examines the role of the contact angle, demonstrated by comparing untreated metallic nozzles with silanized nozzles. Metallic nozzles have  $\theta \approx 0^\circ$ . Silanized nozzles are more hydrophobic with a contact angle of  $\theta \approx 100^\circ$ . For all nozzle sizes, silanized nozzles create smaller hydrogel particles, indicating that the contact angle is a parameter influencing the size of ALG particles.

For estimating the hydrogel size in centrifugal synthesis, Tate's law (eq 3) has been used extensively in the literature.<sup>33,34</sup> Plotting the dimensionless droplet size ( $R_p/R_n$ ) against the Bond ( $Bo$ ) number captures the overall trend shown in Figure 2d–f. However, Tate's law clearly overestimates the droplet size, which emphasizes the need for developing more accurate correlations for estimating  $R_p$ .

All of the experimental data for different nozzle sizes, surface tension, and contact angle values given in Figure 2 can be collapsed onto a single experimental curve, shown in Figure 3, by plotting  $(R_p/R_n)^3/\cos\theta$  vs  $Bo$ . The modified Tate's law in eq 4 (red solid line) overestimates the hydrogel size at all  $Bo$  values in the experimental range as mentioned before. In the literature, it is well known that the radius of a pinched-off droplet ( $R_d$ ) from a dripping nozzle is smaller than the radius of a pendant drop estimated by Tate's law ( $R_{di}$ ) as a smaller pendant droplet remains behind after pinch-off (inset of Figure 3). Harkins and Brown first observed this phenomenon in 1919 while measuring the surface tension of liquid droplets by weighing the pinched-off droplets.<sup>41</sup> They experimentally determined a correction factor ( $\Phi$ ) to Tate's law for a liquid of known density extruded through a nozzle very slowly. They found  $\Phi$  to be independent of the nature of the liquid or the nozzle material and to be dependent only on the nozzle radius ( $R_n$ ) and the volume of the pinched-off droplet ( $V_f = 4\pi R_d^3/3$ ). Lando and Oakley<sup>42</sup> applied linear regression to the experimental results of Harkins and Brown<sup>41</sup> and provided a correlation for  $R_n/V_f^{1/3}$  as a function of  $\Phi$

$$2\pi R_n \gamma = \rho V_f g \Phi \quad (5)$$

Along with the development of digital cameras and goniometers that can accurately determine the size of pendant droplets through curve fitting, the drop weight method was replaced with the pendant droplet method and the Du Nouy ring method that enables more accurate measurements of surface tension.<sup>44</sup> Interest in Harkins and Brown's experimental work was renewed with the development of numerical techniques capable of addressing the pinch-off problem. Yildirim et al.<sup>43</sup> numerically validated the experimental results of Harkins and Brown and proposed an easier to use version given below for low  $We$  and  $Oh$  numbers ( $We < 10^{-7}$  and  $Oh < 10^{-3}$ )

$$\left(\frac{R_{df}}{R_n}\right)^3 = 0.9372Bo^{-1.07} \quad (6)$$

Yildirim et al. also studied the effect of the pinch-off process on the droplet size at large  $We$  and  $Oh$  numbers. In experiments presented in Figures 2 and 3, the  $We$  and  $Oh$  numbers covered were relatively low (cf. Discussion section). Plotting eq 6 provided by Yildirim et al. (solid black line) in Figure 3 provides a better fit than Tate's law (solid red line) in the experimental regime. The improved fit compared with that of Tate's law suggests that the pinch-off process has to be taken into account while predicting  $R_p$ . We also considered the possibility of swelling after impact. In this case, the cross-linked hydrogel size  $R_p$  would be different than the size of the pinched-off droplet,  $R_{df}$ . To investigate swelling, we introduced a swelling/shrinking parameter  $C$  where  $R_p = C \times R_{df}$  into eq 6. The resulting equation is given below

$$\left(\frac{R_p}{R_n}\right)^3 = 0.9372C^3Bo^{-1.07} \quad (7)$$

Equation 7 provides a more general version of eq 6, considering materials that can shrink/swell upon cross-linking. Fitting eq 7 to experimental data in Figure 3 using  $C$  as a fitting parameter resulted in  $C = 0.99$ . We conclude that shrinking/swelling does not play an appreciable role for our canonical sample (2% NaALG).

**Operational Phase Diagram.** The results in the previous section clearly demonstrate that the pinch-off process needs to

be taken into account in centrifugal microparticle synthesis. In this section, we demonstrate the interplay of viscous, inertial, and surface tension stresses on centrifugal hydrogel microparticle synthesis with an operational phase diagram (Figure 4). We define scaling arguments for the *no-dripping to dripping* transition, *dripping to dripping with satellite formation* transition, and *dripping to jetting* transition in the corresponding sections. Using the presented scaling arguments, experimentalists can place themselves in the right operational window and control size distributions.

In the centrifugal process, the extruded NaALG solution can exhibit distinct pinch-off regimes that result in drastically different particle size distributions (Figures 1c–e and 8). As the rotational speed ( $\omega$ ) is increased, the centrifugal acceleration ( $a$ ) driving the flow velocity ( $U$ ) increases and the balance of forces governing the flow is altered. The acceleration,  $a$ , is given by  $a = \omega^2 R_{\text{cent}}$  where  $\omega$  is the rotational speed in rad/s and  $R_{\text{cent}}$  is length of the centrifuge arm. For a low viscosity fluid,  $Oh \ll O(1)$ , the pinch-off behavior is dictated by the balance of surface tension and inertial stress. We observed that hydrogels start dripping into the  $\text{CaCl}_2$  bath above a critical acceleration, which we refer as the *no-dripping to dripping* transition discussed in the Results section. This transition exists because of a balance between the gravitational body force pushing the NaALG solution out of the nozzle and capillary force holding the fluid filament at the nozzle. Once the fluid is extruded from the nozzle, three distinct hydrogel particle size distributions are observed (Figure 1c–e). Spherical monodisperse droplets are formed at low  $a$  values (Figure 1c), indicating that the ALG droplets are extruded as single droplets, and pinch-off behavior is classified as *dripping without satellites*. At intermediate  $a$  values, satellite hydrogel particles with bimodal size distributions appear (Figures 1d and 8). We refer to this pinch-off behavior as *dripping with satellites*. At high  $a$  values, polydisperse hydrogel particles are produced as shown in Figure 1e, suggesting that the fluid is extruded as a single liquid column and breaks into polydisperse droplets either prior to or after impact. At high NaALG concentrations, the viscous effects come into play and alter the centrifugal speeds where the aforementioned pinch-off regimes are observed in Figure 4. Pearl-like morphologies seen at high viscosities are attributed to the jetting liquid column impacting on the liquid bath prior to jet breakup and discussed in detail in the Jet Breakup section. Different morphologies observed and the transitions between each pinch-off regime are summarized in Figure 4b.

**No-Dripping to Dripping Transition.** For dripping to start, the hydrostatic pressure created by the centrifugal motion on the liquid inside of the nozzle and NaALG compartment (Figure 1) should overcome the Laplace pressure. This situation can be represented by a simple pressure balance where the capillary pressure of a hemisphere ( $2\gamma/R_n$ ) is balanced by the hydrostatic pressure ( $\rho a(h + L)$ ) as

$$\frac{2\gamma}{R_n} = \rho a(h + L) \quad (8)$$

For dripping to start, the left-hand side of eq 8 has to be smaller than the right-hand side. Rewriting this equation provides a simple argument for the onset of dripping.

$$Bo \frac{h + L}{2R_n} > O(1) \quad (9)$$

Figure 5 shows results of a set of experiments where  $a$  is gradually increased, and the transition  $a$  at which the first

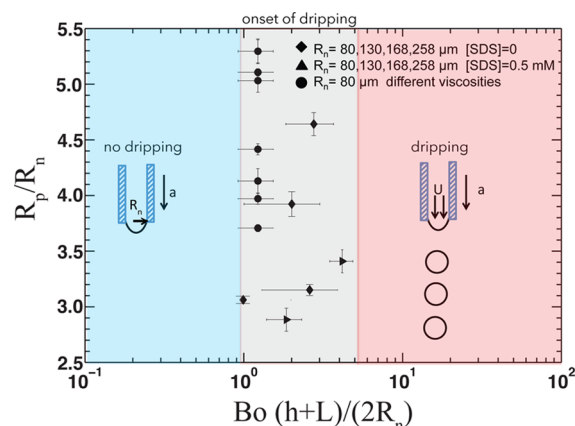


**Figure 5.** Radius of the particle ( $R_p$ ) normalized by the nozzle radius ( $R_n$ ) with respect to the modified Bond number ( $Bo(h + L)/2R_n$ ) is plotted along the no-dripping to dripping transition.

hydrogel dripped is noted. Plotting the results of this experiment with the modified Bond number demonstrates a transition region shown in Figure 5 in accordance with eq 9. We attribute the large error bars to the instrumental inaccuracy in setting  $a$  and contact angle hysteresis.<sup>44</sup> It is important to note that the modified Bond number given in eq 9 has no term accounting for the viscosity of NaALG solutions. This indicates that the *no-dripping to dripping* transition has to be observed at the same  $\omega$  for different NaALG concentrations in Figure 4. Indeed, the operational phase diagram corroborates this prediction. However, longer centrifugation times are required for the observation of dripping in high viscosity NaALG solutions compared to that of low viscosity NaALG solutions with identical  $a$ ,  $R_n$ ,  $h$ , and  $L$  values. At large  $Oh$  values, the observation of this transition is slowed down because of longer travel times of the viscous fluid through the nozzle.

**Dripping without Satellites to Dripping with Satellites Transition.** To identify the *dripping without satellites to dripping with satellites* transition, we followed the experimental procedure described in the Experimental procedure section where the centrifugal acceleration is gradually increased and the resulting hydrogel particles are imaged. The transition is identified as the first centrifugal acceleration  $a$  at which satellite droplets are observed. For a given NaALG solution, at low centrifugal accelerations below this critical value, the nozzle is in the *dripping without satellites* regime and at accelerations above this critical value, satellite droplets emerge.

Figure 4a shows how the acceleration for this transition varies with the viscosity of the ALG solutions. In the *dripping with no satellite* regime, every droplet is detached from the nozzle in a breakup time scale  $\tau_b$  that scales with liquid properties (surface tension  $\gamma$ , density  $\rho$ , and viscosity  $\mu$ ) and the geometry of the nozzle  $R_n$ . Each of these parameters can affect the dynamics of the local flow in the thinning filament that is formed between the pendant drop and the nozzle. In the inviscid case, where viscous stresses are negligible, the imposed pressure from capillary stress leads to the acceleration of liquid elements in the fluid filament, resulting in the drainage of the fluid from the connecting neck into both the hanging drop and the hemispherical cap at the nozzle. Thus, the capillary and inertial forces balance each other, leading to an inertia-capillary

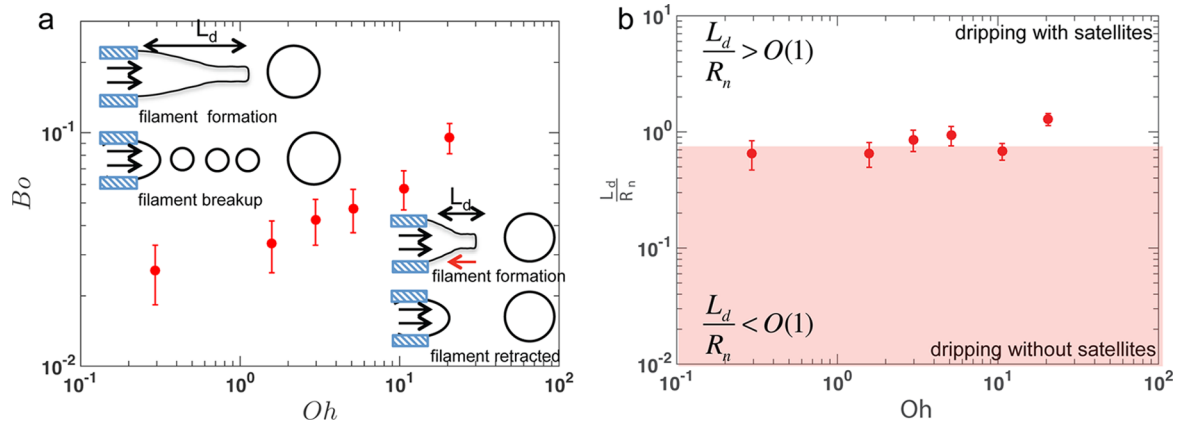


**Figure 6.** (a)  $Bo$  number versus  $Oh$  plotted for data points along the *dripping without satellites* to *dripping with satellites* transition. The data points are taken from Figure 4a. The bottom inset illustrates *dripping without satellites*. After the pinch-off, the remaining filament of length ( $L_d$ ) retracts, that is,  $L_d/R_n < O(1)$ . The top inset illustrates the dripping with satellites. After the pinch-off, satellite droplets are formed. (b) Length of the filament normalized by the radius of the nozzle ( $L_d/R_n$ ) versus  $Oh$  is plotted along the *dripping without satellites* to *dripping with satellites* transition.

balance. For the inviscid case, the breakup time in the nozzle scales with the inertia-capillary time scale  $\tau_b \approx \tau_{cap} \equiv \sqrt{\rho R_n^3 / \gamma}$ .<sup>45–47</sup> This scaling for the breakup time emerges also in the linear stability analysis for an inviscid liquid column.<sup>48,49</sup> In the presence of viscous effects, the local balance between capillary and inertial stresses will be affected by viscous forces. The extra viscous resistance in the liquid thread slows down the thinning dynamics, leading to a longer breakup time for the filament. Several studies in the literature<sup>47,49</sup> show that for a viscous thread linear stability analysis provides a new scaling for the breakup time  $\tau_b \approx \tau_{cap} f(Oh)$ , in which  $f(Oh) = 2\sqrt{2} + 6Oh$  is a linear function of the Ohnesorge number.<sup>39,40</sup> This scaling can be easily derived from the long-wave dispersion relationship that is discussed in detail by Eggers and Villermaux in their review on liquid jets.<sup>47</sup> In the limit of low viscosity, the viscous correction  $f(Oh)$  reaches a constant value  $\lim_{Oh \ll 1} f(Oh) \rightarrow 2\sqrt{2}$ , and we recover the inviscid scaling  $\tau_b \approx \tau_{cap}$ . For very viscous threads, the viscous correction  $f(Oh)$  is linearly proportional to the Ohnesorge number  $\lim_{Oh \gg 1} f(Oh) \rightarrow 6(Oh)$  and the breakup time scales with the visco-capillary time  $\tau_b \approx \tau_{visc.-cap.} \equiv \mu R_n / \gamma$ .

To have a quantitative prediction for the transition acceleration between the aforementioned regimes (dripping with satellite and without satellite formation), we study the process by comparing the relevant time scales. The time needed for each drop to detach from the nozzle is equal to the breakup time scale  $\tau_b = \tau_{cap} f(Oh)$ . As the drop is pinching off from the nozzle, the liquid is delivered into the hanging thread through the nozzle. The time scale for the delivery of fluid scales with the convection time scale in the nozzle  $\tau_{conv.} = R_n / U$  where  $U = \rho a(h + L) R_n^2 / 8\mu L$  is the average liquid velocity inside of the nozzle. For a given liquid, if the fluid elements are delivered faster than the natural rate of droplet breakup (i.e.  $\tau_{conv.} \leq \tau_b$ ), then the satellite-less dripping mechanism cannot anymore support the high rate of fluid delivery. This leads to an increase in the length of the connecting filament between the main drop and the nozzle exit. Consequently, the extended filament goes through a secondary pinch-off process and forms smaller satellite droplets, which follow the trajectory of the main droplet and impact into the  $\text{CaCl}_2$  bath. This simplified view can give us a simple criterion for satellite formation

$$\frac{\tau_{cap} f(Oh)}{\tau_{conv.}} < 1 \rightarrow \text{dripping without satellites}$$

$$\frac{\tau_{cap} f(Oh)}{\tau_{conv.}} > 1 \rightarrow \text{dripping with satellites} \quad (10)$$

This criterion is presented by a comparison between the involved time scales ( $\tau_{cap} f(Oh)$  and  $\tau_{conv.}$ ). By multiplying both time scales with the convection velocity  $U$ , the criterion can be rewritten in terms of the length scales involved in the process

$$\frac{L_d}{R_n} < 1 \rightarrow \text{dripping without satellites}$$

$$\frac{L_d}{R_n} > 1 \rightarrow \text{dripping with satellites} \quad (11)$$

where  $L_d = U\tau_b = U\tau_{cap} f(Oh)$  is the length scale, which describes the extension of the connecting filament between the main drop and the nozzle (the inset image in Figure 6a). Replacing  $L_d$  with  $(\rho a(h + L) R_n^2 / 8\mu L) \sqrt{\rho R_n^3 / \gamma} (2\sqrt{2} + 6\mu / \sqrt{\rho \gamma R_n})$  and using the liquid and geometric properties, for every transition acceleration measured and plotted in Figure 6a in a dimensionless form, one can find the corresponding values of  $L_d/R_n$ . Figure 6b shows another dimensionless representation of the data in Figure 6a by plotting transition values of  $L_d/R_n$  for different ALG solutions at different Ohnesorge numbers. It is clear that above a critical value of  $L_d/R_n \approx O(1)$  satellite formation is observed. Thus, the scaling shown in eq 11 predicts a transition criterion for satellite formation, which is in quantitative agreement with observed trends. This simple scaling suggests that for more viscous liquids the transition between the formation of single-size droplets and stretched filaments (that break into satellite droplets) happens at higher  $We$ . Similar scalings from Hinze and Milbourn in their study of rotary atomization<sup>50</sup> suggest that with increasing  $Oh$  through liquid viscosity,  $\mu$ , the transition between the drop and filament formation happens at higher  $We$ .

**Dripping to Jetting Transition.** The *dripping to jetting* transition is identified as the transition from the formation of individual droplets through dripping (with or without satellites) into the ejection of a liquid jet (Figure 4b and the inset of

Figure 7) out of the nozzle. The transition points are determined experimentally by gradually increasing  $We$  through

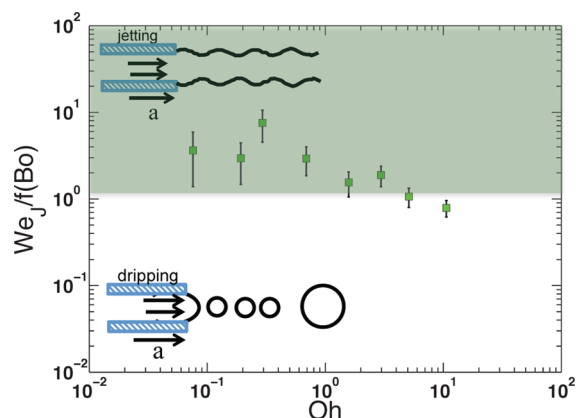


**Figure 7.** Corrected Weber number for jetting ( $We_j$ ) plotted as a function of the Ohnesorge ( $Oh$ ) number along the dripping to jetting transition. The top inset illustrates the jetting phenomenon, and the bottom inset illustrates the *dripping with satellites* regime.

$a$  at fixed  $Oh$  and imaging the resulting hydrogel particles as described in the [Experimental Procedure](#) section. The observation of polydisperse hydrogel size distributions ([Figure 8c,e](#)) is associated with jet breakup prior to impact. The formation of stretched columns with pearl-necklace structures discussed in the [Jet Breakup](#) section is attributed to the fluid jet impacting as a connected single jet into the  $CaCl_2$  bath ([Figure 4b](#)). The *dripping to jetting* transition happens when the momentum of the incoming fluid at the nozzle exit exceeds the resisting capillary pressure. The incoming fluid momentum and the body force on the pendant drop because of centrifugal acceleration favors the transition from dripping to jetting, but

capillary forces resist it. The balance of these three effects can be represented by a combination of critical jetting Weber ( $We_j = \rho U_j^2 R_n / \gamma$ ) and Bond numbers. Clanet and Lasheras<sup>51</sup> showed both by experimental measurements and a theoretical model that the critical Weber number ( $We_j$ ) for the dripping to jetting transition is a function of the Bond number  $f(Bo)$

$$We_j = f(Bo) = 4 \left[ \frac{Bo}{Bo_i} \right]^{1/2} \left[ 1 + \frac{K}{2} (Bo_i Bo)^{1/2} - \left( \left( 1 + \frac{K}{2} (Bo_i Bo)^{1/2} \right)^2 - 1 \right)^{1/2} \right]^2 \quad (12)$$

in which  $Bo_i$  is the Bond number based on the inner nozzle radius and  $Bo$  is the Bond number based on the outer nozzle radius.

This can be rewritten as a criterion for the transition from dripping to jetting

$$\begin{aligned} \frac{We_j}{f(Bo)} &> O(1) \rightarrow \text{jetting} \\ \frac{We_j}{f(Bo)} &< O(1) \rightarrow \text{dripping} \end{aligned} \quad (13)$$

Knowing that  $f(Bo)$  increases with the Bond number and consequently acceleration, one can see that at higher accelerations the transition happens at smaller  $We$ . This shows that in the presence of high acceleration (high  $Bo$ ) the liquid will overcome the capillary pressures with an even smaller initial momentum (smaller  $We$ ). [Figure 7](#) shows the corrected values of the jetting Weber number plotted versus  $Oh$  number. As predicted by the model suggested by Clanet and

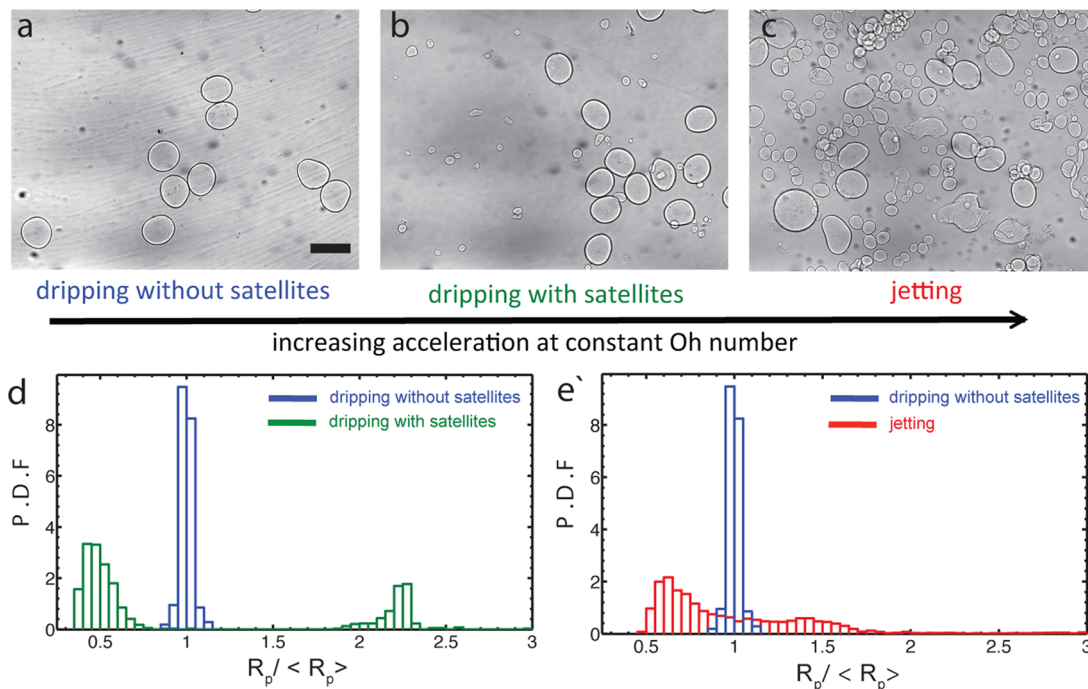


**Figure 8.** Panels a–c show microscopy images of hydrogel particles at different accelerations corresponding to different regimes: (a) *dripping without satellites*, (b) *dripping with satellites*, and (c) *jetting*. The scale bar is 200  $\mu\text{m}$ . Panels d and e show the observed size distributions in different pinch-off regimes. The NaALG concentration is 2.0% ALG corresponding to  $Oh = 0.0145$ .



Lasheras,<sup>51</sup> the critical Weber number for the jetting transition decreases with centrifugal acceleration. Furthermore, in the limit of large accelerations ( $Bo > 1$ ), one can expand eq 12 into  $\lim_{Bo \gg 1} f(Bo) \approx 4(Bo/Bo_i)(K^2 Bo Bo_{ni})^{-2}$ , which scales as  $a^{-2}$ .

Thus, the suggested model by Clanet and Lasheras<sup>51</sup> predicts that the critical Weber number for the dripping to jetting transition scales as  $f(Bo)$  and decreases with acceleration as  $We_j \approx a^{-2}$ . Figure 7 shows a plot of  $We_j/f(Bo)$  values versus Ohnesorge number for all liquids tested in this study. It is clear that the transition from dripping to jetting does not show a recognizable trend with changes in the viscosity over a wide range of Ohnesorge numbers, and within the experimental errors, the transition occurs at a constant value of  $We_j/f(Bo) \approx O(1)$ . Thus, by replacing gravitational acceleration with centrifugal acceleration, a simple model based on the interaction between capillary, inertia, and gravitational effects (suggested by Clanet and Lasheras<sup>51</sup>) can be used to provide an approximate criterion for the transition from dripping to jetting in our rotary configuration (eq 12).

**Jet Breakup.** To understand why the broad hydrogel particle size distributions and pearl-necklace geometries are observed at high accelerations (Figure 1e), we estimate the jet breakup length ( $L_j$ ) using a relationship that is proposed by Middleman<sup>52</sup>

$$\frac{L_j}{2R_n} = 19.5(\sqrt{We_j}(1 + 3Oh))^{0.85} \quad (14)$$

Middleman showed that a Newtonian liquid jet characterized by the corresponding values of Weber and Ohnesorge numbers ( $We_j$  and  $Oh$ ) breaks into a series of droplets in air at a length  $L_j$  away from the nozzle exit described by eq 14. By comparing  $L_j$  to the gap height  $H$  between the nozzle and the  $\text{CaCl}_2$  bath, we can conclude whether the jet breaks up into individual droplets before impacting into the bath ( $L_j \leq H$ ) or it enters the bath as a connected jet ( $L_j > H$ ). One can estimate lower limits for  $L_j$  from eq 14 by inserting the  $We_j$  and  $Oh$  values at the dripping to jetting transition (Figures 4 and 7). The lower estimates for  $L_j$  values vary from  $32R_n$  to  $360R_n$ , whereas the distance  $H$  is kept constant at  $3.6 \text{ mm} \approx 45R_n$ . This simple scaling suggests that in the current geometry, for most liquids, right after the dripping to jetting transition, the jet impacts the bath as a connected column of the liquid, and because of the inertia of the impact, the fragmentation of the liquid column results into a group of individual droplets with a relatively polydisperse size distribution. This explains the polydispersity that is observed for the size distributions in Figures 1e and 8e as well as the cylindrical columns with pearl-necklace geometries that have been observed for high NaALG concentrations shown in Figure 4b. At low NaALG concentrations where  $L_j \approx H$ , jet breaks up prior to/during impact into the liquid bath, and the fragmentation dynamics are faster than those of the gelation process (lower viscous resistance), leading to a polydisperse size distribution observed in Figure 8. At high NaALG concentrations where  $L_j > H$ , the jet impacts onto the liquid bath as a liquid column and the extra resistance from viscous stresses delays the fragmentation process, forming corrugated liquid columns that go through gelation before they break up into individual droplets. Thus, gelation freezes the breakup process in time and creates pearl-necklace morphologies that are observed in Figure 4b.

**Particle Size Distributions.** Figure 8 shows the size distributions of hydrogel particles synthesized at different

pinch-off regimes. Panels a–c show the microscopy images of ALG hydrogel particles corresponding to *dripping without satellites*, *dripping with satellites*, and *jetting* regimes, respectively. The hydrogel droplets shown in Figure 8 are synthesized at a fixed value of the Ohnesorge number  $Oh = 0.0145$  but at different values of centrifugal acceleration  $a$ . Panel d compares the size distributions between two hydrogel particle sets that are prepared in *dripping without satellites* (blue data points) and *dripping with satellites* (green data points) regimes. For hydrogel droplets synthesized in the *dripping with satellites* regime, two distinct peaks are visible in their corresponding size distribution. The satellite droplets are approximately 5 times smaller than the main droplets. Figure 8d compares the corresponding size distribution for hydrogel particles between the *jetting* regime (red data points) and *dripping without satellites* regime (blue data points). It is clear from the size distributions plotted in Figure 8e that the jetting regime leads to relatively broad size distributions, which is a natural outcome for the multi-length-scale and multi-time-scale process of jet fragmentation upon a liquid bath at high Weber numbers.<sup>53</sup>

**Phase Diagram for Centrifugal Synthesis.** For researchers interested in manufacturing hydrogel microparticles, it is helpful to know the limits of different regimes—that are described in our study—within the context of a dimensionless phase diagram. Such a phase diagram for different regimes of pinch-off in the centrifugal synthesis of hydrogel droplets is shown in Figure 9. The dimensional parameters used in Figure

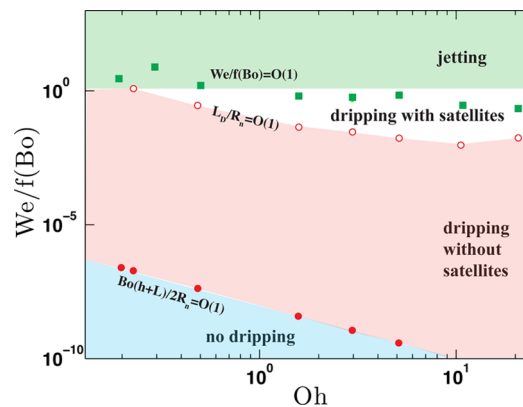


**Figure 9.** Dimensionless phase diagram for centrifugal synthesis.  $We/f(Bo)$  vs  $Oh$  demonstrates the different pinch-off regimes predicted from the scaling arguments and the transitions between them. The experimental points are from Figure 4a.

4a can be replotted in a dimensionless form, developing a phase map in which the transitions between different pinch-off regimes are controlled by the scaling arguments. Figure 9 is a plot of the corrected  $We$  number,  $We/f(Bo)$  versus the Ohnesorge number, and shows the four pinch-off regimes observed in our study separated from each other by the corresponding criteria.

The transition between *no dripping* to *dripping without satellites* is set by the competition between the hydrostatic pressure created by the centrifugal acceleration and the resisting capillary pressure in the pendant drop at the nozzle exit (eq 9). The transition between *dripping without satellites* and *dripping with satellites* is explained by eq 11. The *dripping* to *jetting* transition is governed by the interaction between inertia, capillary, and centrifugal forces and a corrected value of the

Weber number  $We/f(Bo)$  described by eq 13 provides an approximate for this transition.

## DISCUSSION

Our work provides a detailed study of the centrifugal synthesis of hydrogel particles and identifies critical parameters that control the size of synthesized hydrogel particles, as well as different pinch-off regimes governing the corresponding size distributions.

**Previously Overlooked Pinch-Off Regimes & Experimental Parameters.** Previous studies<sup>32–34</sup> observed the emergence of bidisperse or polydisperse particle size distributions, yet a physical description was not provided. Scientists trying to reproduce the reported experiments previously struggled to synthesize monodisperse particles and had to operate by a trial and error methodology. With the scaling arguments provided, experimentalists can now rationally choose operating conditions to be in the desired pinch-off regime and hence achieve monodisperse particle size populations.

Experimental parameters such as the contact angle,  $\theta$ , and the liquid viscosity,  $\mu$ , and geometrical parameters such as the length of the needle,  $L$ , the height of the fluid,  $h$ , and the nozzle to  $\text{CaCl}_2$  bath distance,  $H$ , were not studied systematically in previous studies.<sup>33,34</sup> Our results indicate that these parameters influence the pinch-off regime and particle sizes. For instance, both  $h$  and  $L$  influence the flow speed,  $U$  (eq 2), and hence also affect  $We$  and  $Bo$ . For instance, slightly reducing  $h$  or increasing  $L$  can move an experiment from the *dripping with satellites* regime to the *dripping without satellites* regime, hence avoiding the emergence of satellites.  $H$  is also found to influence the particle shape at low  $We$ . Maeda et al. also observed the formation of asymmetric hydrogel particles with larger  $H$ .<sup>33</sup> We placed the nozzle as close as possible to the  $\text{CaCl}_2$  bath, that is, the smallest  $H$  experimentally accessible to minimize shape deformations. At large  $We$ , a jet is ejected from the nozzle.  $H$  dictates whether this jet will impact the bath before or after the jet breakup (Jet Breakup section). Further details on the geometry of the setup and a detailed discussion of the influence of  $H$  are provided in the Supporting Information.

**Influence of the Pinch-Off Process on the Particle Size.** Previous studies<sup>33,34</sup> relied on Tate's law, which ignores the pinch-off process (eq 3), to estimate the average size of hydrogel particles. Figure 3 demonstrates that Tate's law underestimates the average particle size. We hypothesize that a portion of the pendant drop should stay behind once the pendant droplet pinches off as the volume of the pinched-off droplet is smaller than the volume of the pendant droplet. Along with the proof provided by the phase diagram, we conclude that the pinch-off process needs to be taken into account. The numerical correlation by Yildirim et al. (eq 6) predicts the average droplet size within the experimental regime covered in this study. Equation 6 is only valid for small  $We$  and  $Oh$  where the impact speed on the  $\text{CaCl}_2$  bath is small.<sup>43</sup>

**Influence of Shrinking/Swelling after Impact on the Particle Size.** A droplet of radius  $R_{\text{df}}$  can shrink/swell its size to  $R_{\text{p}}$  upon cross-linking. The degree of cross-linking dictates the extent of swelling/shrinking. Fitting eq 7 where  $C$  is a shrinking/swelling parameter to Figure 3 resulted in  $C \approx 0.99$  for the canonical sample. This result indicates that the pinched-off droplet shrinks slightly yet it is not statistically significant. Therefore, we conclude that the shrinking is not significant for our canonical sample.

We expect shrinking to be more pronounced with higher NaALG concentrations as previously reported in cross-linking with dripping or bulk experiments.<sup>25,26</sup> Furthermore, other cross-linking materials such as chitosan may shrink or swell depending on the formulation and cross-linking solution conditions.<sup>2,4</sup> Therefore, determining  $C$  prior to experiments is important for shrinking/swelling materials. The fitting parameter  $C$  can be determined in simple dripping experiments where the  $R_{\text{df}}$  and  $R_{\text{p}}$  can be measured by video imaging prior to and after impact. Once  $C$  is determined for a given formulation, semiempirical eq 7 can predict the particle size accurately.

**Behavior at Finite  $We$  and  $Oh$  Numbers.** Equation 6 holds within the *dripping without satellites* regime where  $We$  and  $Oh$  are small. However, more accurate correlations considering finite values of  $We$  and  $Oh$  can be developed. Particularly, for large  $Oh$  and  $We$ , we expect deviations from eq 6. Once specific values of  $We$  and  $Oh$  numbers are known, corrections to eq 6 can be introduced using numerical simulations.<sup>54</sup>

**Differences between Dripping Faucet Experiments and Centrifugal Synthesis.** It is important to mention that the experimental system used by Harkins and Brown,<sup>41</sup> the dripping faucet,<sup>55</sup> has fundamental distinctions from the NiC setup used in centrifugal synthesis. In dripping faucet experiments, the average fluid velocity,  $U$ , can be independently controlled by controlling the pumping rate; hence,  $Bo$  and  $We$  are independent of each other. In centrifugal synthesis, both  $Bo$  and  $We$  are dependent on the centrifugal acceleration,  $a$ ; therefore, the numerical solutions of the 1D slender jet equation<sup>56</sup> given in Yildirim et al.<sup>43</sup> for the dripping faucet has to be used with caution. The experiments by Harkins and Brown<sup>41</sup> are dripping faucet experiments with diminishingly small  $We$  numbers, and the  $Bo$  number governed by gravitational acceleration,  $g$ , is constant for a given  $R_{\text{n}}$  and fluid properties. Yildirim et al.<sup>43</sup> provided the numerical solutions connecting  $R_{\text{df}}/R_{\text{n}}$  to  $Bo$  for a given  $We$ , whereas in experiments shown in Figure 3, the  $We$  changes with  $Bo$  and a new numerical solution is required for every  $Bo$ , which is a time-consuming process. For predicting the hydrogel particle size in Figure 3, we utilized the correlations for low  $We$  in eq 6, which does not account for the full coupling of  $Bo$  and  $We$ . In the experiments presented in Figure 3,  $Oh$  varies between 0.15 and 0.25 because of changes in  $R_{\text{n}}$  and  $\gamma$ .  $We$  varies between 0.01 and 0.1. We attribute the variations at high  $Bo > 10^{-1}$  observed in Figure 3 to inertial effects, that is, non-negligible  $We$  numbers.

From a fundamental fluid mechanics point of view, the pinch-off process in the centrifugal synthesis of ALG hydrogels is analogous to the dripping–jetting transition in the flow of a liquid through a nozzle<sup>51,54</sup> yet subtle differences exist. In dripping nozzle studies, the flow rate of the fluid is controlled, whereas the  $Bo$  is defined by the gravitational acceleration and hence is approximately constant. In other words,  $We$  and  $Bo$  numbers can be independently varied. In centrifugal synthesis, the centrifugal acceleration drives the flow and both  $We$  and  $Bo$  depend on  $a$ ; therefore, they are interconnected. The correction given in eq 12 developed by Clarnet and Lasheras<sup>51</sup> becomes more important for centrifugal synthesis because of varying and significantly larger values of  $Bo$ . Furthermore, the impact of the pinched-off droplet and the reaction aspect increases the complexity of experiments compared to the dripping nozzle problem.

**Experimental Issues.** In dripping faucet experiments, the pinch-off process is directly observed, which allows for accurate measurements of droplet shape, size distribution, and exit velocity. In our study, the presented predictions are based on the average hydrogel size and size distributions acquired by image processing after cross-linking. This is due to experimental difficulties in imaging at high centrifugal speeds and the need for developing a dedicated centrifugation apparatus. Haerberle et al. used stroboscopic imaging techniques to visualize the pinch-off process under centrifugal acceleration.<sup>34</sup> We predict that employing stroboscopic imaging techniques in future studies can enable a better insight into the pinch-off process under acceleration.

The non-Newtonian behavior of NaALG solutions also has to be taken into consideration. As demonstrated by Haerberle et al.,<sup>34</sup> the rheological behavior of NaALG solutions gives rise to the formation of very long filaments at large stain rates with concentrated NaALG solutions. For our canonical sample, we did not observe a significant effect of the shear-thinning behavior of NaALG solutions that comes into play at large  $We$  and  $Oh$  numbers. This effect can manifest itself by decreasing the viscosity and increasing  $U$  at a given  $Bo$ , therefore inducing jetting at lower  $a$  values than predicted in eq 12 where  $We$  is calculated using zero shear viscosity.

## CONCLUSIONS

Centrifugal synthesis of hydrogel particles is a promising microparticle synthesis method. It enables the rapid manufacturing of relatively large quantities of hydrogel particles with standard lab equipment. Despite its promise, the lack of a physical understanding of the method has limited its widespread use. Previous studies predicted an average droplet size using a simple force balance over a pendant drop, ignoring the pinch-off process. Furthermore, the observations of non-monodisperse particle size distributions were not connected to different pinch-off regimes.<sup>33,34</sup>

In this study, we improved the overall physical understanding of the centrifugal hydrogel synthesis method. We provided a correlation taking into account the pinch-off phenomenon for predicting the average size of hydrogel particles accurately within the *dripping without satellites* regime at low  $We$  and  $Oh$  numbers. Furthermore, we explained the emergence of different pinch-off regimes (*dripping without satellites*, *dripping with satellites*, and *jetting*) governing size distributions and presented scaling arguments predicting the transition between regimes. Our systematic study unveiled the importance of previously overlooked parameters and connected them to pinch-off regimes. The presented results can guide the rational design of centrifugal synthesis hydrogels and polymeric particles for various applications.

## ASSOCIATED CONTENT

### Supporting Information

The Supporting Information is available free of charge on the ACS Publications website at DOI: 10.1021/acs.langmuir.6b00806.

Guide for experimentalist: design of a nozzle-in-centrifuge (NiC) apparatus, influence of the distance between the nozzle and the liquid bath on the particle shape, density of NaALG as a function of NaALG concentration, surface tension of NaALG with SDS, and hydrophobization of nozzles (PDF)

## AUTHOR INFORMATION

### Corresponding Author

\*E-mail: pdoyle@mit.edu.

### Author Contributions

#H.B.E., E.R.S., and B.K. contributed equally.

### Notes

The authors declare no competing financial interest.

## ACKNOWLEDGMENTS

This work was supported by the MIT-Novartis Center for Continuous Manufacturing. ERS acknowledges the Lord Foundation for the MIT undergraduate researcher opportunity program. The content of the information does not necessarily reflect the position or the policy of the Government, and no official endorsement should be inferred.

## REFERENCES

- (1) Abernethy, C. D.; Codd, G. M.; Spicer, M. D.; Taylor, M. K. A highly stable *N*-heterocyclic carbene complex of trichloro-oxovanadium(V) displaying novel Cl–C(carbene) bonding interactions. *J. Am. Chem. Soc.* **2003**, *125*, 1128–1129.
- (2) Celiz, A. D.; Smith, J. G. W.; Langer, R.; Anderson, D. G.; Winkler, D. A.; Barrett, D. A.; Davies, M. C.; Young, L. E.; Denning, C.; Alexander, M. R. Materials for stem cell factories of the future. *Nat. Mater.* **2014**, *13*, 570–579.
- (3) Hennink, W. E.; van Nostrum, C. F. Novel crosslinking methods to design hydrogels. *Adv. Drug Delivery Rev.* **2012**, *64*, 223–236.
- (4) Langer, R.; Tirrell, D. A. Designing materials for biology and medicine. *Nature* **2004**, *428*, 487–492.
- (5) Lee, J.; Bisso, P. W.; Srinivas, R. L.; Kim, J. J.; Swiston, A. J.; Doyle, P. S. Universal process-inert encoding architecture for polymer microparticles. *Nat. Mater.* **2014**, *13*, 524–529.
- (6) Helgeson, M. E.; Chapin, S. C.; Doyle, P. S. *Curr. Opin. Colloid Interface Sci.* **2011**, *16*, 106–117.
- (7) Kraft, D. J.; Groenewold, J.; Kegel, W. K. Colloidal molecules with well-controlled bond angles. *Soft Matter* **2009**, *5*, 3823–3826.
- (8) Sacanna, S.; Pine, D. J.; Yi, G.-R. Engineering shape: the novel geometries of colloidal self-assembly. *Soft Matter* **2013**, *9*, 8096–8106.
- (9) Dendukuri, D.; Doyle, P. S. The Synthesis and Assembly of Polymeric Microparticles Using Microfluidics. *Adv. Mater.* **2009**, *21*, 4071–4086.
- (10) Park, J. I.; Saffari, A.; Kumar, S.; Günther, A.; Kumacheva, E. Microfluidic Synthesis of Polymer and Inorganic Particulate Materials. *Annu. Rev. Mater. Res.* **2010**, *40*, 415–443.
- (11) Teh, S.-Y.; Lin, R.; Hung, L.-H.; Lee, A. P. Droplet microfluidics. *Lab Chip* **2008**, *8*, 198–220.
- (12) Dendukuri, D.; Pregibon, D. C.; Collins, J.; Hatton, T. A.; Doyle, P. S. Continuous-flow lithography for high-throughput microparticle synthesis. *Nat. Mater.* **2006**, *5*, 365–369.
- (13) Yang, S.-M.; Kim, S.-H.; Lim, J.-M.; Yi, G.-R. Synthesis and assembly of structured colloidal particles. *J. Mater. Chem.* **2008**, *18*, 2177–2190.
- (14) Whitesides, G. M.; Grzybowski, B. Self-assembly at all scales. *Science* **2002**, *295*, 2418.
- (15) Uspal, W. E.; Eral, H. B.; Doyle, P. S. Engineering particle trajectories in microfluidic flows using particle shape. *Nat. Commun.* **2013**, *4*, 2666.
- (16) Kraft, D. J.; Ni, R.; Smallenburg, F.; Hermes, M.; Yoon, K.; Weitz, D. A.; van Blaaderen, A.; Groenewold, J.; Dijkstra, M.; Kegel, W. K. Surface roughness directed self-assembly of patchy particles into colloidal micelles. *Proc. Natl. Acad. Sci. U.S.A.* **2012**, *109*, 10787–10792.
- (17) Mastrobattista, E.; van der Aa, M. A. E. M.; Hennink, W. E.; Crommelin, D. J. A. Artificial viruses: a nanotechnological approach to gene delivery. *Nat. Rev. Drug Discovery* **2006**, *5*, 115–121.

- (18) Hackelbusch, S.; Seiffert, S. *In Situ Gelling Polymers*; Loh, X. J., Ed.; Series in BioEngineering; Springer: Singapore, 2015; pp 151–185.
- (19) Tomme, S. R. V.; Storm, G.; Hennink, W. E. In situ gelling hydrogels for pharmaceutical and biomedical applications. *Int. J. Pharm.* **2008**, *355*, 1–18.
- (20) Drury, J. L.; Mooney, D. J. Hydrogels for tissue engineering: scaffold design variables and applications. *Biomaterials* **2003**, *24*, 4337–4351.
- (21) Lee, K. Y.; Mooney, D. J. Alginate: Properties and biomedical applications. *Prog. Polym. Sci.* **2012**, *37*, 106–126.
- (22) Lacy, P.; Hegre, O.; Gerasimidi-Vazeou, A.; Gentile, F.; Dionne, K. Maintenance of normoglycemia in diabetic mice by subcutaneous xenografts of encapsulated islets. *Science* **1991**, *254*, 1782–1784.
- (23) Ching, S. H.; Bansal, N.; Bhandari, B. Alginate gel particles—a review of production techniques and physical properties. *Crit. Rev. Food Sci. Nutr.* **2015**, *48*, 100–110.
- (24) Hu, Y.; Wang, Q.; Wang, J.; Zhu, J.; Wang, H.; Yang, Y. Shape controllable microgel particles prepared by microfluidic combining external ionic crosslinking. *Biomicrofluidics* **2012**, *6*, 026502.
- (25) Eral, H. B.; Lopez-Mejias, V.; O'Mahony, M.; Trout, B. L.; Myerson, A. S.; Doyle, P. S. Biocompatible Alginate Microgel Particles as Heteronucleants and Encapsulating Vehicles for Hydrophilic and Hydrophobic Drugs. *Cryst. Growth Des.* **2014**, *14*, 2073–2082.
- (26) Eral, H. B.; O'Mahony, M.; Shaw, R.; Trout, B. L.; Myerson, A. S.; Doyle, P. S. Composite Hydrogels Laden with Crystalline Active Pharmaceutical Ingredients of Controlled Size and Loading. *Chem. Mater.* **2014**, *26*, 6213–6220.
- (27) Rolland, L.; Santanach-Carreras, E.; Delmas, T.; Bibette, J.; Bremond, N. Physicochemical properties of aqueous core hydrogel capsules. *Soft Matter* **2014**, *10*, 9668–9674.
- (28) Zhang, H.; Tumarkin, E.; Peerani, R.; Nie, Z.; Sullan, R. M. A.; Walker, G. C.; Kumacheva, E. Microfluidic Production of Biopolymer Microcapsules with Controlled Morphology. *J. Am. Chem. Soc.* **2006**, *128*, 12205–12210.
- (29) Bonhomme, O.; Leng, J.; Colin, A. Microfluidic wet-spinning of alginate microfibers: a theoretical analysis of fiber formation. *Soft Matter* **2012**, *8*, 10641–10649.
- (30) Haerberle, S.; Zengerle, R.; Ducrée, J. Centrifugal generation and manipulation of droplet emulsions. *Microfluid. Nanofluid.* **2007**, *3*, 65–75.
- (31) Mark, D.; Haerberle, S.; Zengerle, R.; Ducree, J.; Vladisavljevic, G. T. Manufacture of chitosan microbeads using centrifugally driven flow of gel-forming solutions through a polymeric micronozzle. *J. Colloid Interface Sci.* **2009**, *336*, 634–641.
- (32) Lee, J.; Kim, J. Multiphasic Sensory Alginate Particle Having Polydiacetylene Liposome for Selective and More Sensitive Multi-targeting Detection. *Chem. Mater.* **2012**, *24*, 2817–2822.
- (33) Maeda, K.; Onoe, H.; Takinoue, M.; Takeuchi, S. Controlled Synthesis of 3D Multi-Compartmental Particles with Centrifuge-Based Microdroplet Formation from a Multi-Barrelled Capillary. *Adv. Mater.* **2012**, *24*, 1340–1346.
- (34) Haerberle, S.; Naegele, L.; Burger, R.; von Stetten, F.; Zengerle, R.; Ducrée, J. Alginate bead fabrication and encapsulation of living cells under centrifugally induced artificial gravity conditions. *J. Microencapsulation* **2008**, *25*, 267–274.
- (35) Rabaud, D.; Thibault, P.; Mathieu, M.; Marmottant, P. Acoustically Bound Microfluidic Bubble Crystals. *Phys. Rev. Lett.* **2011**, *106*, 134501.
- (36) Wagner, C.; Amarouchene, Y.; Bonn, D.; Eggers, J. Droplet Detachment and Satellite Bead Formation in Viscoelastic Fluids. *Phys. Rev. Lett.* **2005**, *95*, 164504.
- (37) Li, L.; Fang, Y.; Vreeker, R.; Appelqvist, I.; Mendes, E. Reexamining the Egg-Box Model in Calcium–Alginate Gels with X-ray Diffraction. *Biomacromolecules* **2007**, *8*, 464–468.
- (38) Deen, W. M. *Analysis of Transport Phenomena*; Oxford: 2011.
- (39) Ohnesorge, W. V. Die Bildung von Tropfen an Düsen und die Auflösung flüssiger Strahlen. *J. Appl. Math. Mech.* **1936**, *16*, 355–358.
- (40) McKinley, G. H.; Renardy, M. Wolfgang von Ohnesorge. *Phys. Fluids* **2011**, *23*, 127101.
- (41) Harkins, W. D.; Brown, F. E. The determination of surface tension (free surface energy), and the weight of falling drops: The surface tension of water and benzene by the capillary height method. *J. Am. Chem. Soc.* **1919**, *41*, 499–524.
- (42) Lando, J. L.; Oakley, H. T. Tabulated correction factors for the drop-weight-volume determination of surface and interracial tensions. *J. Colloid Interface Sci.* **1967**, *25*, 526–530.
- (43) Yildirim, O. E.; Xu, Q.; Basaran, O. A. Analysis of the drop weight method. *Phys. Fluids* **2005**, *17*, 062107.
- (44) Eral, H. B.; 't Mannetje, D. J. C. M.; Oh, J. M. Contact angle hysteresis: a review of fundamentals and applications. *Colloid Polym. Sci.* **2013**, *291*, 247–260.
- (45) Rayleigh, L. On the capillary phenomenon of jets. *Proc. R. Soc. London* **1879**, *29*, 71–97.
- (46) Eggers, J. Nonlinear dynamics and breakup of free-surface flows. *Rev. Mod. Phys.* **1997**, *69*, 865–930.
- (47) Eggers, J.; Villermaux, E. Physics of liquid jets. *Rep. Prog. Phys.* **2008**, *71*, 036601.
- (48) Rayleigh, L. On the instability of jets. *Proc. London Math. Soc.* **1878**, *10*, 4–13.
- (49) Chandrasekhar, S. *Hydrodynamic and Hydromagnetic Stability*; Dover Publications: 1961; p 652.
- (50) Hinze, J. O.; Milborn, H. Atomization of liquids by means of a rotating cup. *Journal of Applied Mechanics-Transactions of ASME* **1950**, *17*, 145–153.
- (51) Clanet, C.; Lasheras, J. C. Transition from dripping to jetting. *J. Fluid Mech.* **1999**, *383*, 307–326.
- (52) Middleman, S. Stability of a viscoelastic jet. *Chem. Eng. Sci.* **1965**, *20*, 1037–1040.
- (53) Villermaux, E. Fragmentation. *Annu. Rev. Fluid Mech.* **2007**, *39*, 419–446.
- (54) Notz, P. K.; Basaran, O. A. Dynamics and breakup of a contracting liquid filament. *J. Fluid Mech.* **2004**, *512*, 223–256.
- (55) Ambravaneswaran, B.; Subramani, H. J.; Phillips, S. D.; Basaran, O. A. Dripping-jetting transitions in a dripping faucet. *Phys. Rev. Lett.* **2004**, *93*, 034501.
- (56) Eggers, J.; Dupont, T. Drop formation in a one-dimensional approximation of the Navier–Stokes equation. *J. Fluid Mech.* **1994**, *262*, 205.